Nano World Journal

https://doi.org/10.17756/nwj.2023-s4-096

Research Article

Open Access

Influence of Silica Nanoparticles on Structural, Electrical, and Dielectric Properties of PEO/PVdF/$NaNO_3$/EC Based Composite Solid Polymer Electrolytes

Malla Reddy Yalla[1*], Venakata Ramana Jeedi[2], S. Shashi Devi[3], Kiran Kumar Ganta[2], S. Narender Reddy[4] and A. Sadananda Chary[5]

[1]*Department of Physics, University P.G. College, Osmania University, Hyderabad, Telangana, India*
[2]*Department of Physics, B.V. Raju Institute of Technology, Narsapur, Telangana, India*
[3]*Vardhaman College of Engineering, Hyderabad, Telangana, India*
[4]*Stanley College of Engineering and Technology for Women, Hyderabad, Telangana, India*
[5]*Department of Physics, University College of Science, Osmania University, Hyderabad, Telangana, India*

[*]Correspondence to:
Malla Reddy Yalla
Department of Physics,
University P.G. College,
Osmania University,
Hyderabad, Telangana, India.
E-mail: mahi.yalla@gmail.com

Received: September 19, 2023
Accepted: December 11, 2023
Published: December 13, 2023

Citation: Yalla MR, Jeedi VR, Devi SS, Ganta KK, Reddy SN, et al. 2023. Influence of Silica Nanoparticles on Structural, Electrical, and Dielectric Properties of PEO/PVdF/$NaNO_3$/EC Based Composite Solid Polymer Electrolytes. *NanoWorld J* 9(S4): S562-S569.

Copyright: © 2023 Yalla et al. This is an Open Access article distributed under the terms of the Creative Commons Attribution 4.0 International License (CCBY) (http://creativecommons.org/licenses/by/4.0/) which permits commercial use, including reproduction, adaptation, and distribution of the article provided the original author and source are credited.

Published by United Scientific Group

Abstract

Solid polymer electrolytes (SPEs) have attracted greater attention for various technological applications such as fuel cells, sensors, photochemical solar cells, super-capacitors, and electrochromic display devices. The main advantages of SPEs are good electrochemical stability, safety, flexibility, and durability. However, SPEs have limitations due to their poor conductivity at ambient temperature. In this context, many researchers have explored various methods to enhance the ionic conductivity by taking blended SPEs, plasticized-SPEs, nanocomposite-SPEs and plasticized-nanocomposite SPEs during the last few decades. In this study, composite solid polymer electrolyte systems (CSPEs) were developed by combining polyethylene oxide (PEO) and polyvinylidene fluoride (PVdF) is host polymer matrix. The solution casting method was used to prepare CSPEs using sodium nitrate ($NaNO_3$) salt as an ion dopant, ethylene carbonate (EC) as a plasticizer and silicon dioxide (SiO_2) as a nanofiller. X-ray diffraction (XRD), Fourier transform infrared spectroscopy (FTIR), differential scanning calorimetry (DSC) and scanning electron microscopy (SEM) were used to characterize the CSPEs. Impedance spectroscopy was used to investigate the electrical, dielectric, and electric modulus properties of the CSPEs between temperatures of 298 K and 343 K. The maximum ionic conductivity measured using impedance study was found to be 8 wt.% SiO_2 nanofiller. It was attributed to the addition of SiO_2 increasing the amorphous nature and conducting paths. The ionic transport number was calculated using Wagner's polarization method.

Keywords

Composite solid polymer electrolyte, X-ray diffraction, Scanning electron microscope, Differential scanning calorimetry, Impedance analysis, Nanofiller, Ionic conductivity

Introduction

Nanotechnology involves manipulating matter on an atomic or molecular scale, typically at the nanometer scale. It's a multidisciplinary field that merges science and engineering, aiming to understand, control, and utilize materials and devices at the nanoscale. Nano-engineered materials have enhanced properties, like increased strength, conductivity, or flexibility, which find applications in various industries from aerospace to construction. Lithium-ion batteries are prominent among the numerous energy storage devices available because of their favorable commercial applications [1-3]. However, the high cost, diminishing

abundance, environmental and health issues associated with lithium materials hinder their future use of battery improvements [4]. As a result, an alternative energy storage device is required to compensate for the lithium battery. Sodium-ion batteries have received much attention due to their low cost, environmental friendliness, non-toxicity, and material availability. The thermoplastic polymer PEO is extensively used in battery development due to its versatile mechanical properties. In 1975, Peter V. Wright noticed that PEO could serve as a host for Na and K salts, causing in a steady solid polymer electrolyte [5]. The crystalline nature is the main disadvantage for the movement of the ions in PEO-based SPEs [6].

To reduce crystallinity, several co-polymer matrices can be used in place of a single polymer as the base matrix. As a result, for multifunctional devices, new blended polymer electrolyte materials with probable physicochemical, optical, and dielectric properties are being developed [7-10]. Combining PEO with other polymers is becoming increasingly appealing in the preparation of all potential SPE materials [11-14]. The semi crystalline polar PVdF has better physicochemical and electroactive properties. Hence it has been used in several blended polymer systems [15, 16]. The miscibility of PEO and PVdF blending was reported by [17].

Plasticizers can increase the mobility of the polymer segment by making the polymer-salt complex more amorphous. EC and propylene carbonate (PC) appear to be important among several plasticizers that have been found to improve conductivity in polymer electrolytes. Between EC and PC, EC would be the better plasticizer due to its less viscosity compared to PC, which results in better mobility of polymer segments [18].

The incorporation of nanofillers such as Al_2O_3, Fe_2O_3, SnO_2, ZrO_2, silicon dioxide (SiO_2) and others, has been shown to be an active method for increasing in ionic conductivity of electrolyte materials with improved thermomechanical durability. All synthesis methods described above are crucial for improving the properties of various electrochemical applications [19, 20]. Because of their high strength, admirable durability, significant corrosion resistance and acidic environment resistance, SiO_2 is widely used in polymer nanocomposite-based nano dielectrics. Since the permittivity of SiO_2 is comparable to that of different polymers, SiO_2 is used as nanofiller in this work [21, 22]. The impact of SiO_2 nanoparticles on the plasticized blend polymer matrix has been studied through the structural and electrical properties of the resultant electrolyte material.

Experimentation

PEO (M_w = 2,00,000), PVdF (M_w = 2,70,000), $NaNO_3$ (M_w = 84.99), EC (M_w = 88.06) and SiO_2 (size = 10 - 20 nm) and dimethyl formamide were procured from Sigma Aldrich. CSPEs have been synthesized as 80 PEO/20 PVdF/5 $NaNO_3$/5 EC/xSiO_2 (where x = 0, 2, 4, 6, 8, 10, and 12 wt.%) by solution casting method. PEO, PVdF, $NaNO_3$, EC, and SiO_2 are dissolved in 50 ml of dimethyl formamide with the help of a magnetic stirrer keeping a break of an hour between every chemical dissolution. The entire solution was heated for 2 h at 60 °C. Stirring continued for another 36 h to achieve a homogeneous solution, which was poured into a petri dish and dried for 48 h at 60 °C. The processed systems were labeled and stored in a desiccator as described in table 1.

Results and Discussion

XRD studies

Figure 1 represents the XRD configurations of the pure PEO, PVdF, $NaNO_3$, EC, SiO_2 and different wt.% of SiO_2 dispersed CSPEs. The peaks at 19.08°, 23.1° and 23.52° are related to pure PEO, which is characteristic of the crystalline host polymer. The broader peaks at 38.9° and 20.22° indicate the semi crystalline nature of α and β phases of pure PVdF respectively and are correlated to the earlier reported results [23, 24]. A broad hump observed in the XRD configurations indicates the amorphous nature of pure SiO_2. The characteristic peak of $NaNO_3$ at 29.11° has disappeared in all PPNES systems, which confirms the complexation of salt in all CSPEs. The peaks that appeared around 19° and 23° in all PPNES systems correspond to the un-complexed PEO. The peak widening progressively increases and shifts to lower-angles as SiO_2 nanofiller is loaded to PPNES-0 up to 8 wt.%. This can be due to SiO_2 nanoparticles interacting with the host polymer matrix, leading to the structural reformation of the host polymer electrolyte systems [25]. The size of crystallite has been evaluated using Scherrer's formula for all PPNES systems and is shown in table 1. The lowest crystallite size noticed for the PPNES-8 system indicates the attainment of a highly amorphous nature compared to all other compositions.

Table 1: System code, composition ratio, XRD parameters and crystallite size of various CSPEs.

System code	PEO:PVdF:$NaNO_3$:EC:SiO_2	2θ (Degree)	FWHM	Crystallite size (nm)
PPNES-0	80:20:05:05:00	22.76	0.80	10.16
PPNES-2	80:20:05:05:02	23.17	0.72	11.21
PPNES-4	80:20:05:05:04	23.08	0.76	10.68
PPNES-6	80:20:05:05:06	23.05	0.76	10.60
PPNES-8	80:20:05:05:08	22.70	0.86	9.45
PPNES-10	80:20:05:05:10	23.04	0.79	10.27
PPNES-12	80:20:05:05:12	23.03	0.77	10.57

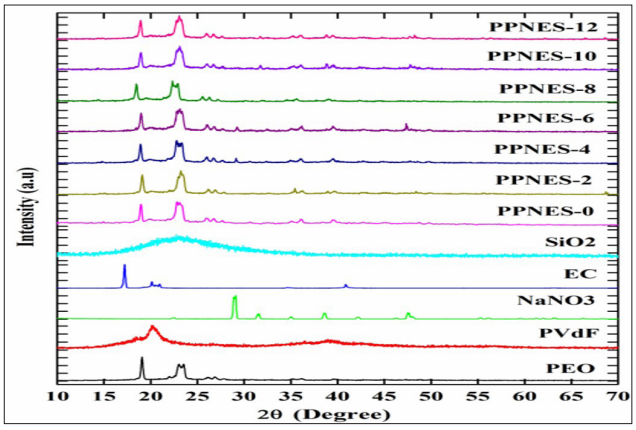


Figure 1: XRD patterns of pure base materials and SiO_2 dispersed CSPEs.

FTIR studies

FTIR has been carried out to investigate the functional groups present in composite polymer electrolytes dispersed with SiO_2. The interaction between atoms or ions in the electrolyte system causes a change in molecular vibration modes. The FTIR spectra of PPNES systems with SiO_2 dispersed electrolyte membranes are shown in figure 2. A peak around 3417 cm^{-1} in all PPNES systems is ascribed to the stretching hydroxyl group (O-H). The peaks at 511 cm^{-1}, 841 cm^{-1} and 1384 cm^{-1} are allocated to the respective γ, β, and α phases of PVdF [24]. The asymmetric vibrations of CH_2 of PVdF are noticed at 2850 cm^{-1}. PEO's C=O stretching mode vibrations have been observed at 1751 cm^{-1} [26]. The C=O stretching vibrations around 1630 cm^{-1} confirm the plasticizer (EC) presence in all PPNES systems. The peak at 664 cm^{-1} is assigned to contact ion pair with PEO/PVdF blend polymer. It is observed from the figure that the peak of the contact ion pair (664 cm^{-1}) shifted slightly towards lower frequency by increasing the nanofiller concentration suggesting higher dis-sociability of sodium salt [27]. A peak at 1698 cm^{-1} corresponds to the interaction between sodium cation and C-O group of blend polymer, which shift to lower frequency as filler content increases. This shows that there is an interaction between sodium cation and carbonyl group existing in all PPNES systems.

DSC studies

DSC is an essential tool to analyze the thermal properties of materials. DSC thermograms of pure form of PEO, PVdF, EC and composite polymer-electrolytes with different concentrations of SiO_2 have been shown in figure 3. The endothermic peaks at 65.2 °C and 41.6 °C correspond to PEO and EC melting temperatures (T_m), respectively. The melting temperatures of all PPNES systems decrease nearly 5 °C upon adding SiO_2 nanofiller up to 8 wt.%. The lowest T_m (59.8 °C) was noticed for PPNES-8 system. The decrease in T_m could be due to the orientation of polymer chains caused by the interaction between SiO_2 nanofiller and polymer segments [28]. The glass transition temperature is usually less than T_m and is a measure of polymer chains flexibility, which increases as the T_m decreases. A decrease in the value of T_m helps increase the movements of polymer chains, which enhances the conductivity of polymer electrolytes [29]. It is also observed that the endothermic peak of PPNES-8 is more broadened than all other PPNES systems. The sharp to broad melting point conversion clearly shows the rise in the amorphous phase of the PPNES-8 system.

SEM studies

Figure 4 illustrates the SEM images of CSPEs with and without nanofiller at 2.5 kx magnifications. It is observed from figure 4a that the surface of PPNES-0 (without nanofiller) system has many variable sizes with distinct boundaries of the amorphous regions. When 2 wt.% of SiO_2 nanofiller is added to PPNES-0, it can be seen from figure 4b; small size balloon-shaped spherulites have been formed, which are frequently isolated from each other by the surrounding large amorphous regions. As the filler content increases up to 6 wt.%, the balloon-shaped spherulite size increases along with

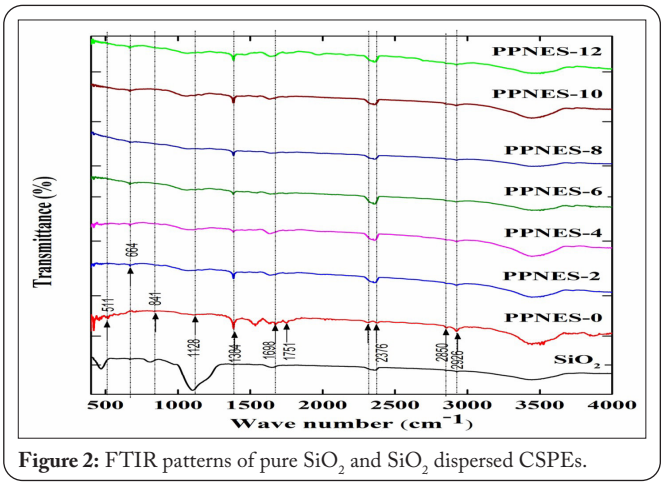


Figure 2: FTIR patterns of pure SiO_2 and SiO_2 dispersed CSPEs.

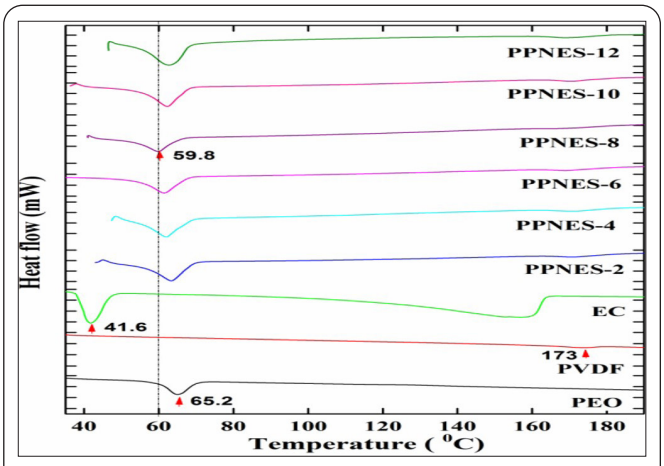


Figure 3: DSC patterns of pure base materials and SiO_2 dispersed CSPEs.

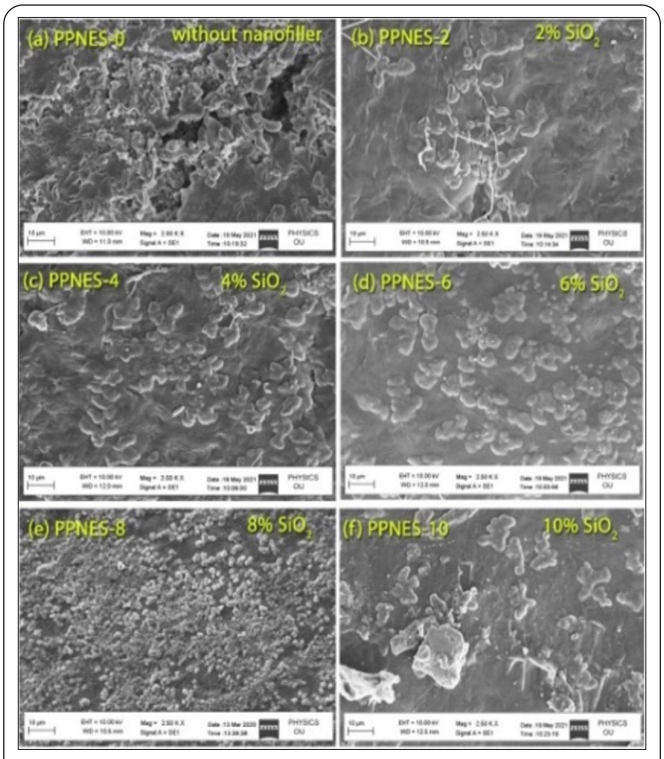


Figure 4: SEM images of **(a)** PPNES-0 (without nanofiller), **(b)** PPNES-2, **(c)** PPNES-4, **(d)** PPNES-6, **(e)** PPNES-8, and **(f)** PPNES-10.

a decrease in surrounding amorphous regions shown in figure 4c and 4d [30]. A large number of small spherulites have overlapped for the 8 wt.% SiO_2 composition, demonstrating the good compatibility of nanoparticles with a high degree of homogeneity. The SiO_2 nanoparticles in the PPNES-8 system are distributed uniformly, confirming the formation of admirable nanocomposites as shown in figure 4e [31].

Impedance studies

Complex impedance measurements at various temperatures have been carried out from 100 Hz to 10 MHz to understand the impact of SiO_2 nanofiller on the ionic conductivity of CSPE systems. Figure 5a depicts the complex impedance plots of various SiO_2 concentrations of CSPEs at room temperature. It is observed from the figure that the existence of semicircle in all PPNES systems in the higher frequency region and a spike at an angle-less than 90° in the lower-frequency region indicates that all the systems are partially resistive and capacitive. The intercept of extrapolated semicircle on the X-axis (real Z') provides the bulk resistance (R_b) of the CSPE systems [32]. As the SiO_2 nanofiller wt.% increases, the R_b decreases up to 8 wt.%. The lowest R_b noticed for the PPNES-8 system could be due to the many charge carriers present and increased movement of ions. The increase in bulk resistance above 8 wt.% is attributed to ion-ion interaction, which causes ion species to aggregate, causing in the formation of ion-clusters, which restricts charge carrier movement.

The impedance plots of the PPNES-8 system at different temperatures are shown in figure 5b. It is observed from figure 5b that the intercept of the semicircle on the X-axis moves towards the origin as the temperature increases resulting in the growth of ionic conductivity, which could be attributed to the rise in ion dissociation.

DC ionic conductivity

The DC ionic conductivity has been evaluated from the complex impedance plot using relation $\sigma_{dc} = \frac{t}{AR_b}$, where 't' is thickness, 'A' is area of cross-section of the CSPE systems and is shown in table 2. The ionic conductivity with inverse temperature plots for all PPNES systems has been displayed in figure 6. It has been noticed that the ionic conductivities of PPNES-2 and PPNES-4 are lower than that of PPNES-0. This may be due to the blockage of the existing conductive pathways and the possible aggregation of low-weight percent silica, thereby reducing the polymer-filler interface. When the silica content increases to more than 4 wt.%, then the surface charge layer formed at the polymer/filler-interface provides a conductive path for sodium ions, the conductive path again generates up to 8 wt.%. Further increase in filler content leads to blockage and termination of conductive pathways [33]. The activation-energy (E_a) has been evaluated using slopes obtained from log σ vs 1000/T plot and the E_a values are listed in table 2. It can be noticed that PPNES-8 system has the lowest E_a, which corresponds to the highest ionic conductivity (2.107×10^{-4} S cm^{-1}) compared to all other systems.

AC conductivity

Figure 7a depicts the variation of AC-conductivity with the frequency of different PPNES systems at room temperature. This can be understood by dividing the frequency response into three different characteristic regions. In the low-frequency area, the conductivity slightly increases with frequency due to a slight decrease in the space charge polarization. The frequency-independent DC conductivity in the

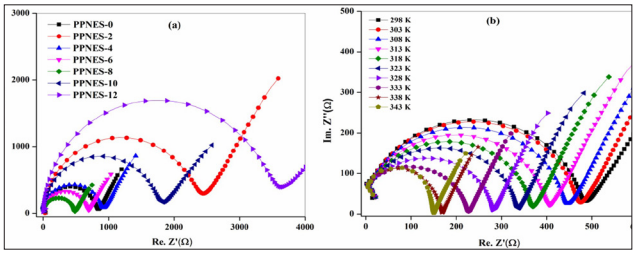


Figure 5: Complex impedance plots of **(a)** SiO_2 dispersed CSPEs at room temperature and **(b)** PPNES-8 at various temperatures.

Table 2: Activation energy, ionic conductivity, and ion transport number of various CSPEs.

System code	Activation energy E_a (eV)	Ionic conductivity (S cm^{-1})	Ion transport number (T_{ion})
PPNES-0	0.468	1.275×10^{-4}	0.93
PPNES-2	0.489	4.561×10^{-5}	0.88
PPNES-4	0.452	1.119×10^{-4}	0.90
PPNES-6	0.419	1.344×10^{-4}	0.94
PPNES-8	0.412	2.107×10^{-4}	0.96
PPNES-10	0.463	5.465×10^{-5}	0.89
PPNES-12	0.512	5.694×10^{-5}	0.86

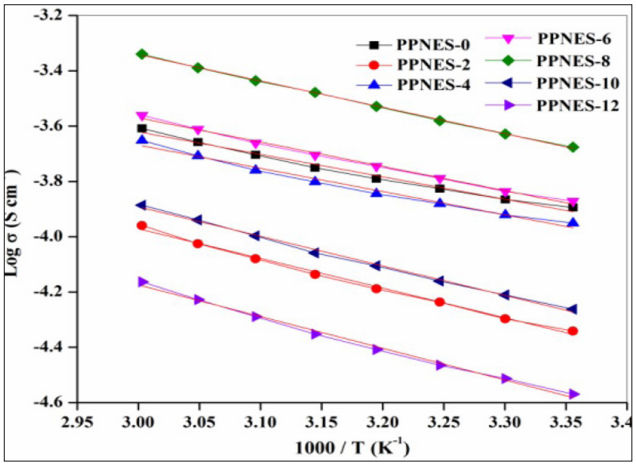


Figure 6: Arrhenius plot: Log σ vs 1000/T.

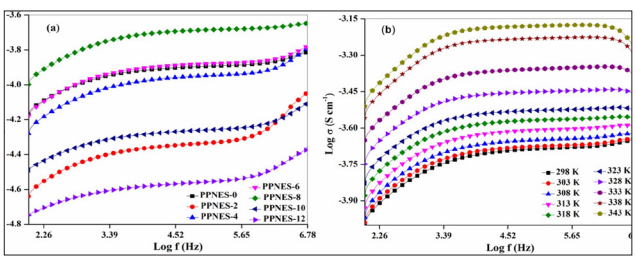


Figure 7: Frequency dependent conductivity of **(a)** SiO_2 dispersed CSPEs at room temperature and **(b)** PPNES-8 at various temperatures.

intermediate frequency area could be ascribed to the absence of space charge polarization and mobility of free charges. In the high-frequency dispersion area, conductivity increases abruptly with the rise of frequency due to the short-range ion mobility and dipole relaxation. In general, conductivity follows the customary Jonscher power law [34]. From figure 7a, it can be seen that PPNES-8 system has the highest conductivity among all CSPE systems. PPNES-8 is the optimum- conducting composition in the current study. Figure 7b depicts the variation of PPNES-8 system AC conductivity with frequency at various temperatures. It has been observed that the conductivity is independent of frequency, even in the high-frequency region at higher temperatures. At higher temperatures, the increased plateau region is a characteristic feature of nanocomposite polymer electrolytes arising out of thermally activated processes.

Dielectric constant and loss tangent

The frequency dependent dielectric constant (ε') of various PPNES systems at ambient temperature is depicted in figure 8a. It can be observed that ε' spectra show dispersion at lower frequency. The high value of ε' at lower frequency, ascribed to electrode/electrolyte and space charge polarization decreases exponentially with frequency. In the low frequency area, ions move towards the blocking electrodes when an external electric field is applied but cannot be transported to the external circuit. As a result, ions become trapped near the electrode/electrolyte interface, forming a heterogeneous charge layer. As the frequency increases, ε' drops sharply and finally reaches a saturation value in the high frequency area because, the ion cannot follow the fast periodic orientation of the applied field [35]. It can be seen that PPNES-8 shows a high ε' at room temperature concerning all other systems. Figure 8b illustrates the temperature-dependent ε' of PPNES-8. From the figure, the ε' values of PPNES-8 system were observed to increases with rise in temperature. This could be due to the expansion of the free volume in the polymer matrix. This allows more rotational freedom for the polarization of the polymer chain dipolar groups, resulting in a larger value of ε' [36].

Figure 9a illustrates the frequency-dependence of dielectric loss (ε'') of different PPNES systems at ambient temperature. The ε'' followed the similar behavior as that of ε' in all PPNES systems. At lower frequencies, there is a plentiful time for charges to accumulate at the boundary before the electric-field reversal, resulting in a large apparent value of ε'' which is the maximum for PPNES-8 system. As the frequency increases, charges do not have enough time to accumulate at the interface, resulting in decreased ε'' [37, 38]. Figure 9b shows the temperature-dependent ε'' of PPNES-8 system at various temperatures. It is observed from the figure, as the temperature increases the ε'' rises due to an increase in motion of free ions at the interface. High temperatures can resist the formation of ion aggregation and clustering in the polymer-matrix resulting in high ε'' [39, 40].

The variation of loss tangent (tan) of all PPNES systems as a function of frequency at 298 K are shown in figure 10a. The relation between loss-tangent in terms of ε' and ε'' is given by tan $\delta = (\varepsilon''/\varepsilon')$ and indicates the proportion of electric energy lost to energy stored. The figure shows that the tan δ rises with frequency, approaches a maximum value at the resonance frequency (f_r), and decreases rapidly above f_r. The maximum loss tangent has been noticed for the PPNES-8 system, which shifted most towards higher frequency than all other systems. The relaxation time can be calculated by $\tau = 1/(2\pi f_r)$, where f_r is the resonance frequency corresponding to the relaxation-peak. The expression shows clearly that the peak f_r is inversely proportional to the ion's relaxation time. The variation of tan δ of PPNES-8 with temperature has been displayed in figure 10b. As the temperature of the polymer electrolyte rises, the peak position moves towards a higher frequency. As a result, the relaxation time decreases. This could be due to thermally generated imperfections in the polymer electrolyte that cause the significant value of loss tangent at high temperatures [41, 42].

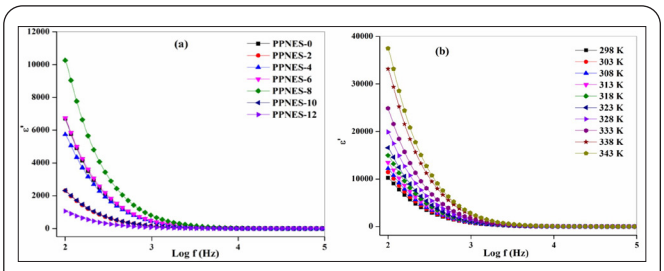


Figure 8: Discrepancy of dielectric constant with frequency **(a)** SiO_2 dispersed CSPEs at room temperature and **(b)** PPNES-8 at various temperatures.

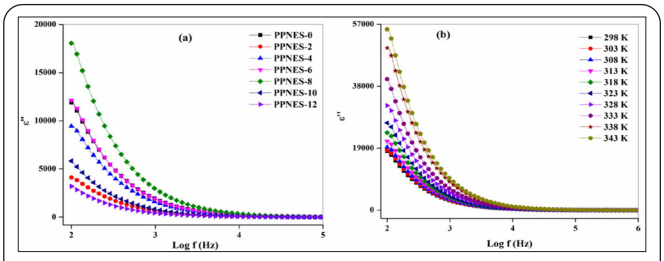


Figure 9: Variation of dielectric loss with the frequency of **(a)** SiO_2 dispersed CSPEs at room temperature and **(b)** PPNES-8 at various temperatures.

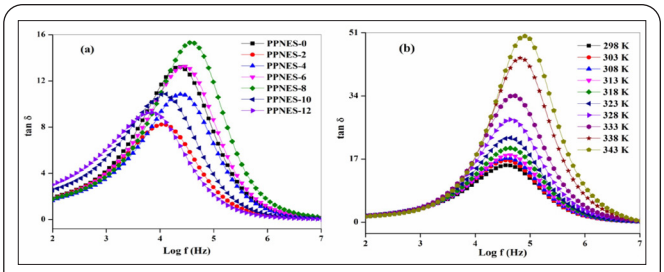


Figure 10: Variation of tan δ with the frequency of **(a)** SiO_2 dispersed CSPEs at room temperature and **(b)** PPNES-8 at various temperatures.

Electric modulus studies

Figure 11a depicts the variation of real modulus (M') of all PPNES systems with frequency at room temperature. M' of all the systems can be noticed to shift to higher frequency region by enhancing the wt.% of SiO_2 up to 8 wt.%. In the lower frequency area, the M' values of all PPNES seems to be steady up to 10^4 Hz and become non-linear from 10^4 Hz

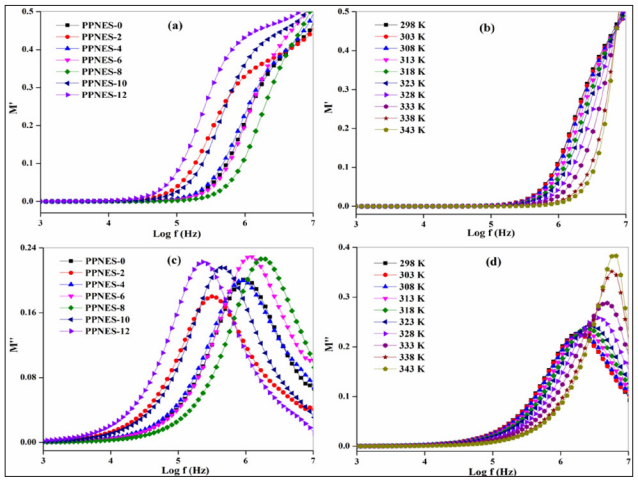


Figure 11: The frequency variation of **(a)** real electric modulus of SiO_2 dispersed CSPEs at room temperature, **(b)** real electric modulus of PPNES-8 at various temperatures, **(c)** imaginary electric modulus of SiO_2 dispersed CSPEs at room temperature, and **(d)** imaginary electric modulus of PPNES-8 at various temperatures.

to 10 MHz. From figure 11b, the M' dispersion can be shifted towards higher frequency with an increase in temperature. The sudden rise in M′ not only indicates the absence of electrode polarization and the onset of the hopping mechanism [43, 44]. Figure 11c and 11d represent the variation of imaginary modulus (M″) of all PPNES systems with frequency at room temperature and optimum composition (PPNES-8) at various temperatures respectively. Due to the insignificant contribution of electrode polarization, the imaginary part of the electric modulus in the low-frequency range is approaching zero. The values of M″ rise with frequency and reach a maximum at a specific frequency which could be due to long-range random hopping of ions in the material. The ionic relaxation process in polymer electrolytes, where long-range motion is constrained to caged motion, is attributed to the peaks observed in M″ spectra at higher frequency [45, 46]. The wider and asymmetric peaks in M″ spectrum can be assigned to the non-Debye behavior. As the temperature of the polymer electrolyte rises, the peak location changes to a higher frequency, as shown in figure 11d. This could be due to the fast charge carrier movement resulting in a shorter relaxation time [47, 48].

Ion transport number

Wagner's polarization technique has been used to evaluated the ion transport number for all CSPE systems. The transport number is defined as the ion conductivity to total conductivity ratio. By applying a constant voltage to two stainless steel electrodes, the system was trapped and polarized. The total primary current (i_T) is due to both ions and electrons. The final current (i_e) after prolonged hours of polarization is only from electronic contribution. The electronic transference number (t_e) is evaluated as $t_e = \frac{i_e}{i_T}$ and the ionic transference number is calculated as $t_i = 1 - t_e$. The evaluated values are shown in table 2. PPNES-8 system has the highest ionic transference number compared to all other systems.

Conclusion

SiO_2 nanofiller dispersed composite solid polymer electrolytes are synthesized by solution-cast method with varying nanofiller wt.%. According to XRD results, the amorphous area increased up to 8 wt.% with the addition of SiO_2 and then decreased. The results of the DSC and FTIR studies could be correlated with those of the XRD. Electrical and dielectric studies confirmed the structural reformation of the polymer electrolyte materials. The optimum conducting composition was found to be 8 wt.% of nanofiller, resulting in a maximum enhancement in ionic conductivity, dielectric constant, and maximum ion mobility. In composite polymer electrolyte systems, the addition of SiO_2 nanofiller significantly increases the number of free ions and charge carrier mobility.

Acknowledgements

The authors would like to thank the Department of Physics, Osmania University, Hyderabad for providing an experimental facility.

Conflict of Interest

None.

References

1. Scrosati B, Hassoun J, Sun YK. 2011. Lithium-ion batteries. A look into the future. *Energy Environ Sci* 4(9): 3287-3295. https://doi.org/10.1039/c1ee01388b
2. Korthauer R. 2018. Areas of Activity on the Fringe of Lithium-Ion Battery Development, Production, and Recycling. In Korthauer R (eds) Lithium-Ion Batteries: Basics and Applications. Springer, Berlin, pp 249-251.
3. Liu B, Zhang JG, Xu W. 2018. Advancing lithium metal batteries. *Joule* 2(5): 833-845. https://doi.org/10.1016/j.joule.2018.03.008
4. Karmakar A, Ghosh A. 2012. Dielectric permittivity and electric modulus of polyethylene oxide (PEO)–$LiClO_4$ composite electrolytes. *Curr Appl Phys* 12(2): 539-543. https://doi.org/10.1016/j.cap.2011.08.017
5. Wright PV. 1975. Electrical conductivity in ionic complexes of poly(ethylene oxide). *Br Polym J* 7(5): 319-327. https://doi.org/10.1002/pi.4980070505
6. Xue Z, He D, Xie X. 2015. Poly(ethylene oxide)-based electrolytes for lithium-ion batteries. *J Mater Chem A* 3(38): 19218-19253. https://doi.org/10.1039/c5ta03471j
7. Abdelghany AM, Abdelrazek EM, Badr SI, Morsi MA. 2016. Effect of gamma-irradiation on (PEO/PVP)/Au nanocomposite: materials for electrochemical and optical applications. *Mater Des* 97: 532-543. https://doi.org/10.1016/j.matdes.2016.02.082
8. Choudhary S, Sengwa RJ. 2018. ZnO nanoparticles dispersed PVA–PVP blend matrix based high performance flexible nanodielectrics for multifunctional microelectronic devices. *Curr Appl Phys* 18(9): 1041-1058. https://doi.org/10.1016/j.cap.2018.05.023
9. Choudhary S. 2018. Characterization of amorphous silica nanofiller effect on the structural, morphological, optical, thermal, dielectric and electrical properties of PVA–PVP blend based polymer nanocomposites for their flexible nanodielectric applications. *J Mater Sci Mater Electron* 29(12): 10517-10534. https://doi.org/10.1007/s10854-018-9116-y
10. Zhao X, Zhang W, Chen S, Zhang J, Wang X. 2012. Hydrophilicity and crystallization behavior of PVDF/PMMA/TiO_2 (SiO_2) composites prepared by *in situ* polymerization. *J Polym Res* 19: 9862. https://doi.org/10.1007/s10965-012-9862-0

11. Patla SK, Ray R, Asokan K, Karmakar S. 2018. Investigation of ionic conduction in PEO–PVDF based blend polymer electrolytes. *J Appl Phys* 123(12): 125102. https://doi.org/10.1063/1.5022050
12. Wang X, Hao X, Hengjing Z, Xia X, Tu J. 2020. 3D ultraviolet polymerized electrolyte based on PEO modified PVDF-HFP electrospun membrane for high-performance lithium-sulfur batteries. *Electrochim Acta* 329: 135108. https://doi.org/10.1016/j.electacta.2019.135108
13. Arya A, Sadiq M, Sharma AL. 2018. Effect of variation of different nanofillers on structural, electrical, dielectric, and transport properties of blend polymer nanocomposites. *Ionics* 24: 2295-2319. https://doi.org/10.1007/s11581-017-2364-7
14. Arya A, Sharma AL. 2019. Temperature and salt-dependent dielectric properties of blend solid polymer electrolyte complexed with LiBOB. *Macromol Res* 27: 334-345. https://doi.org/10.1007/s13233-019-7077-5
15. Martins P, Lopes AC, Lanceros-Mendez S. 2014. Electroactive phases of poly(vinylidene fluoride): determination, processing and applications. *Prog Polym Sci* 39(4): 683-706. https://doi.org/10.1016/j.progpolymsci.2013.07.006
16. Lee YY, Liu YL. 2017. Crosslinked electrospun poly(vinylidene difluoride) fiber mat as a matrix of gel polymer electrolyte for fast-charging lithium-ion battery. *Electrochim Acta* 258: 1329-1335. https://doi.org/10.1016/j.electacta.2017.11.191
17. Mohamadi M, Garmabi H, Papila M. 2016. Effect of miscibility state on crystallization behavior and polymorphism in crystalline/crystalline blends of poly(vinylidene fluoride)/poly (ethylene oxide). *Macromol Res* 24: 698-709. https://doi.org/10.1007/s13233-016-4099-0
18. Kumar GG, Munichandraiah N. 2000. Effect of plasticizers on magnesium-poly(ethyleneoxide) polymer electrolyte. *J Electroanal Chem* 495(1): 42-50. https://doi.org/10.1016/S0022-0728(00)00404-6
19. Wang YJ, Kim D. 2007. Crystallinity, morphology, mechanical properties and conductivity study of *in situ* formed PVdF/$LiClO_4$/TiO_2 nanocomposite polymer electrolytes. *Electrochim Acta* 52(9): 3181-3189. https://doi.org/10.1016/j.electacta.2006.09.070
20. Azizi Samir MAS, Alloin F, Gorecki W, Sanchez JY, Dufresne A. 2004. Nanocomposite polymer electrolytes based on poly(oxyethylene) and cellulose nanocrystals. *J Phys Chem B* 108(30): 10845-10852. https://doi.org/10.1021/jp0494483
21. Zhao M, Ren ZZ, Yang MB, Yang W. 2019. Effects of modified nano-silica on the microstructure of PVDF and its microporous membranes. *J Polym Res* 26: 28. https://doi.org/10.1007/s10965-018-1681-5
22. Deshmukh K, Ahamed MB, Sadasivuni KK, Ponnamma D, Al-Maadeed MAA, et al. 2017. Fumed SiO_2 nanoparticle reinforced biopolymer blend nanocomposites with high dielectric constant and low dielectric loss for flexible organic electronics. *J Appl Polym Sci* 134(5): 44427. https://doi.org/10.1002/app.44427
23. Mohanty HS, Kumar A, Kulriya PK, Thomas R, Pradhan DK. 2019. Dielectric/ferroelectric properties of ferroelectric ceramic dispersed poly(vinylidene fluoride) with enhanced β-phase formation. *Mater Chem Phys* 230: 221-230. https://doi.org/10.1016/j.matchemphys.2019.03.055
24. Mallaiah Y, Jeedi VR, Swarnalatha R, Raju A, Reddy SN, et al. 2021. Impact of polymer blending on ionic conduction mechanism and dielectric properties of sodium based PEO-PVdF solid polymer electrolyte systems. *J Phys Chem Solids* 155: 110096. https://doi.org/10.1016/j.jpcs.2021.110096
25. Praveen D, Bhat SV, Damle R. 2013. Role of silica nanoparticles in conductivity enhancement of nanocomposite solid polymer electrolytes:(PEG_xNaBr):ySiO_2. *Ionics* 19: 1375-1379. https://doi.org/10.1007/s11581-013-0871-8
26. Choudhary S, Sengwa RJ. 2017. Effects of different inorganic nanoparticles on the structural, dielectric and ion transportation properties of polymers blend based nanocomposite solid polymer electrolytes. *Electrochim Acta* 247: 924-941. https://doi.org/10.1016/j.electacta.2017.07.051
27. Manjuladevi R, Thamilselvan M, Selvasekarapandian S, Mangalam R, Premalatha M, et al. 2017. Mg-ion conducting blend polymer electrolyte based on poly(vinyl alcohol)-poly(acrylonitrile) with magnesium perchlorate. *Solid State Ionics* 308: 90-100. https://doi.org/10.1016/j.ssi.2017.06.002
28. Kumar M, Sekhon SS. 2002. Role of plasticizer's dielectric constant on conductivity modification of PEO–NH_4F polymer electrolytes. *Eur Polym J* 38(7): 1297-1304. https://doi.org/10.1016/S0014-3057(01)00310-X
29. MacFarlane DR, Sun J, Meakin P, Fasoulopoulos P, Hey J, et al. 1995. Structure-property relationships in plasticized solid polymer electrolytes. *Electrochim Acta* 40(13-14): 2131-2136. https://doi.org/10.1016/0013-4686(95)00152-5
30. Dhatarwal P, Sengwa RJ. 2019. Impact of PVDF/PEO blend composition on the β-phase crystallization and dielectric properties of silica nanoparticles incorporated polymer nanocomposites. *J Polym Res* 26(8): 196. https://doi.org/10.1007/s10965-019-1859-5
31. Choudhary S. 2018. Structural, morphological, thermal, dielectric, and electrical properties of alumina nanoparticles filled PVA–PVP blend matrix-based polymer nanocomposites. *Polym Compos* 39(S3): E1788-E1799. https://doi.org/10.1002/pc.24793
32. Ganta KK, Jeedi VR, Kumar KV, Narsaiah EL. 2021. Preparation, characterization and impedance spectroscopic studies of Na^+ ion conducting PEO+PVDF-blended polymer electrolytes. *Int J Polym Anal Charact* 26(2): 130-144. https://doi.org/10.1080/1023666X.2020.1860396
33. Abdullah A, Abdullah SZ, Ali AMM, Winie T, Yahya MZA, et al. 2009. Electrical properties of PEO–$LiCF_3SO_3$–SiO_2 nanocomposite polymer electrolytes. *Mater Res Innov* 13(3): 255-258. https://doi.org/10.1179/143307509X440451
34. Ganta KK, Jeedi VR, Katrapally VK, Yalla M, Emmadi LN. 2021. Effect of TiO_2 nano-filler on electrical properties of Na^+ ion conducting PEO/PVDF based blended polymer electrolyte. *J Inorg Organomet Polym Mater* 31: 3430-3440. https://doi.org/10.1007/s10904-021-01947-w
35. Howell FS, Bose RA, Macedo PB, Moynihan CT. 1974. Electrical relaxation in a glass-forming molten salt. *J Phys Chem* 78(6): 639-648. https://doi.org/10.1021/j100599a016
36. Choudhary S. 2017. Structural and dielectric properties of (PEO–PMMA)–SnO_2 nanocomposites. *Compos Commun* 5: 54-63. https://doi.org/10.1016/j.coco.2017.07.004
37. Aziz SB. 2013. Li^+ ion conduction mechanism in poly(ε-caprolactone)-based polymer electrolyte. *Iran Polym J* 22(12): 877-883. https://doi.org/10.1007/s13726-013-0186-7
38. Nithya H, Selvasekarapandian S, Kumar DA, Sakunthala A, Hema M, et al. 2011. Thermal and dielectric studies of polymer electrolyte based on P(ECH-EO). *Mater Chem Phys* 126(1-2): 404-408. https://doi.org/10.1016/j.matchemphys.2010.10.047
39. Verma ML, Sahu HD. 2015. Ionic conductivity and dielectric behavior of PEO-based silver ion conducting nanocomposite polymer electrolytes. *Ionics* 21(12): 3223-3231. https://doi.org/10.1007/s11581-015-1517-9
40. Liew CW, Ramesh S, Durairaj R. 2012. Impact of low viscosity ionic liquid on PMMA–PVC–LiTFSI polymer electrolytes based on AC-impedance, dielectric behavior, and HATR–FTIR characteristics. *J Mater Res* 27(23): 2996-3004. https://doi.org/10.1557/jmr.2012.343
41. Choudhary S, Sengwa RJ. 2011. Dielectric relaxation spectroscopy and ion conduction in poly(ethylene oxide)-blend salts-montmorillonite nanocomposite electrolytes. *Indian J Pure Appl Phys* 49(3): 204-213.
42. Kumar TV, Chary AS, Bhardwaj S, Awasthi AM, Reddy SN. 2013. Dielectric relaxation, ionic conduction and complex impedance studies on $NaNO_3$ fast ion conductor. *Int J Mater Sci Appl* 2(6): 173-178. https://doi.org/10.11648/j.ijmsa.20130206.12
43. Teodorescu M, Bercea M, Morariu S. 2019. Biomaterials of PVA and PVP in medical and pharmaceutical applications: perspectives and challenges. *Biotechnol Adv* 37(1): 109-131. https://doi.org/10.1016/j.biotechadv.2018.11.008

44. Mathioudakis GN, Patsidis AC, Psarras GC. 2014. Dynamic electrical thermal analysis on zinc oxide/epoxy resin nanodielectrics. *J Therm Anal Calorim* 116: 27-33. https://doi.org/10.1007/s10973-013-3510-8

45. Kumar M, Srivastava N. 2015. Conductivity and dielectric investigation of NH_4I-doped synthesized polymer electrolyte system. *Ionics* 21: 1301-1310. https://doi.org/10.1007/s11581-014-1294-x

46. Ramlli MA, Isa MIN. 2015. Conductivity study of carboxyl methyl cellulose solid biopolymer electrolytes (SBE) doped with ammonium fluoride. *Res J Recent Sci* 3(6): 59-66.

47. Aziz SB, Abidin ZHZ, Arof AK. 2010. Influence of silver ion reduction on electrical modulus parameters of solid polymer electrolyte based on chitosan-silver triflate electrolyte membrane. *Express Polym Lett* 4: 300-310.

48. Dutta A, Sinha TP, Jena P, Adak S. 2008. AC conductivity and dielectric relaxation in ionically conducting soda–lime–silicate glasses. *J Non Cryst Solids* 354(33): 3952-3957. https://doi.org/10.1016/j.jnoncrysol.2008.05.028